Spectrochimica Acta Part A 83 (2011) 120–129

Contents lists available at ScienceDirect

Spectrochimica Acta Part A: Molecular and Biomolecular Spectroscopy

journal homepage: www.elsevier.com/locate/saa

Application of comparative vibrational spectroscopic and mechanistic studies in analysis of fisetin structure

Jasmina M. Dimitrić Marković[a,*], Zoran S. Marković[b], Dejan Milenković[c], Svetlana Jeremić[b]

[a] Faculty of Physical Chemistry, University of Belgrade, Studentski trg 12-16, 11000 Belgrade, Serbia
[b] Department of Bio-Chemical and Medical Sciences, State University of Novi Pazar, Vuka Karadžića bb, 36300 Novi Pazar, Serbia
[c] Bioengineering Research and Development Center, 34000 Kragujevac, Serbia

ARTICLE INFO

Article history:
Received 16 June 2011
Received in revised form 29 July 2011
Accepted 2 August 2011

Keywords:
Fisetin
IR and Raman spectra
Comparative analysis of the spectra
M05-2X-6-311+G (2df, p) level of theory

ABSTRACT

This paper addresses experimental and theoretical research in fisetin (2-(3,4-dihydroxyphenyl)-3,7-dihydroxychromen-4-one) structure by means of experimental IR and Raman spectroscopies and mechanistic calculations. Density Functional Theory calculations, with M05-2X functional and the 6-311+G (2df, p) basis set implemented in the Gaussian 09 package, are performed with the aim to support molecular structure, vibrational bands' positions and their intensities. Potential energy distribution (PED) values and the description of the largest vibrational contributions to the normal modes are calculated. The most intense bands appear in the 1650–1500 cm^{-1} wavenumber region. This region involves a combination of the C═O, C2═C3 and C–C stretching vibrational modes. Most of the bands in the 1500–1000 cm^{-1} range involve C–C stretching, O–C stretching and in-plane C–C–H, C–O–H, C–C–O and C–C–C bending vibrations of the rings. The region below 1000 cm^{-1} is characteristic to the combination of in plane C–C–C–H, H–C–C–H, C–C–C–C, C–C–O–C and out of plane O–C–C–C, C–C–O–C, C–C–C–C torsional modes. The Raman spectra of baicalein and quercetin were used for qualitative comparison with fisetin spectrum and verification of band assignments. The applied detailed vibrational spectral analysis and the assignments of the bands, proposed on the basis of fundamentals, reproduced the experimental results with high degree of accuracy.

1. Introduction

Flavonoid family is the vast and very important group of low-molecular weight plant phenolics found ubiquitously in plants. Structurally they are benzo-γ-pyrone derivatives built upon a C_6H_5(A)–C_3–C_6H_5(B) flavone skeleton in which oxygen is the heteroatom [1,2].

The unique electron-rich and highly conjugated chemical structure of flavonoids, especially flavones and flavonols, enable them to act as very good hydrogen and electron donors which are very important determinants in antioxidant activity. Their numerous beneficial actions, which include: antitumor activity, the ability to inhibit certain enzymes, detoxification of hydrogen peroxide through non-enzymatic defense mechanisms, pigmentation, nitrogen fixation, termination of the propagation phase in which hydro-peroxy lipids are formed, growth and reproduction, regulation of iron channels associated with phosphorylation, resistance to pathogens and predators, chemical defense and UV-protection of plants, are closely related to their pronounced antioxidant potential [2–19].

The ways to disclose the relationship between the structure, properties and performance of flavonoids as very important molecules are provided, more and more frequently, by combination of experimental measurements and the various tools of computational chemistry. This paper is a part of ongoing investigations of flavonoids' molecular structures [20–22] and it addresses experimental and theoretical research in fisetin structure by means of experimental IR and Raman spectroscopies and mechanistic calculations. Because of its specific structural features fisetin is considered as a potent antioxidant that is consequently arising great medical interest in it. Among its most striking and diverse collection of activities are stimulation of the signaling pathways that enhance long-term memory, neuroprotective role, modulation of the expression of more than twenty genes at transcription level, inhibition of the aggregation of the amyloid beta protein (Abeta) that may cause the progressive neuronal loss in Alzheimer's disease and induction of neuronal differentiation. Recently this has lead to the creation of a new type of therapeutic drug for Alzheimer's disease [23,24]. The applied combination of the experimental vibrational spectroscopic methods and theoretical calculations, could be generally applied in analyzing the structural changes of naturally

* Corresponding author. Tel.: +381 11 333 6624; fax: +381 11 218 7133.
E-mail address: markovich@ffh.bg.ac.rs (J.M. Dimitrić Marković).

1386-1425/$ – see front matter © 2011 Elsevier B.V. All rights reserved.
doi:10.1016/j.saa.2011.08.001

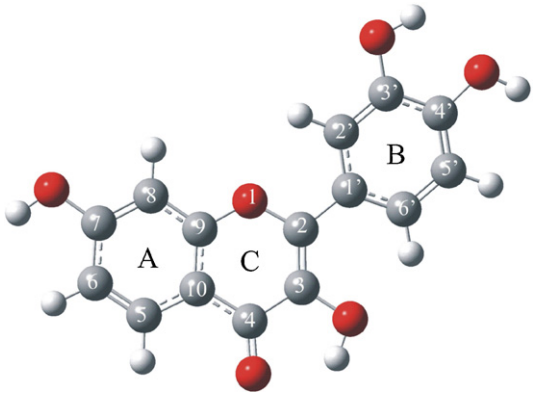

Fig. 1. Structure and atomic numbering of fisetin.

occurring flavonoids under physiologically relevant conditions, providing insight into the mechanism of their bioactivity.

2. Experimental

2.1. Computational methods

The conformations of the most stable fisetin form (Fig. 1) were fully optimized with M05-2X method developed by the Truhlar group [25] by using the 6-311+G (2df, p) basis set as implemented in the Gaussian 09 package [26]. This hybrid meta exchange–correlation functional is parameterized so that it includes both nonmetallic and metallic compounds. This functional yields satisfactory overall performance for the main-group thermochemistry and thermochemical kinetics, as well as organic, organometallic, biological and noncovalent interactions [25,27,28].

The vibrational frequencies were obtained from diagonalization of the corresponding M05-2X Hessian matrices. The nature of the stationary points was determined by analyzing the number of imaginary frequencies: 0 for minimum and 1 for transition state. Relative energies were calculated at 298 K.

The vibrational modes were assigned on the basis of PED analysis using VEDA 4 program with its visualization interface [29]. Normal coordinate analysis of fisetin was carried out to obtain a more complete description of the molecular motions involved in the fundamentals. The calculated vibrational wavenumbers were scaled with the scale factor of 0.9444 in order to obtain better match between calculated and experimental wavenumber values.

Potential energy surface was obtained in relation to the torsion angle τ, defined by the C3–C2–C1′–C2′ atoms, between the rings B and C. The natural bond orbital (NBO) analysis [30–33] of fiestin was also performed.

2.2. IR spectra

IR spectra were recorded on a Thermo Nicolet 6700 FT-IR Spectrometers with ATR. The spectra were recorded in the middle IR region, 4000–400 cm^{-1}, which is important for monitoring the structural changes of molecule. The spectral resolution was 2 cm^{-1}. Fisetin (Merck, USA) was studied in potassium bromide matrix with a ratio of 1 mg:150 mg (fisetin:KBr).

2.3. Raman spectra

Raman spectra were recorded on Thermo Scientific Nicolet Almega XR Raman spectrometer. A 532 nm laser was used for sample illumination, enabling a spectral resolution of 2 cm^{-1}. The spectrum of solid phase was recorded at room temperature by using the potassium bromide matrix (1 mg:150 mg; fisetin:KBr). Each spectrum was collected after 1 s of exposure. The number of exposures was ten. The fluorescence correction has been done.

The theoretical Raman intensities (I_i^R) were derived from the computed Raman scattering activities using the following equations:

$$I_i^R = C(\upsilon_0 - \upsilon_i)^4 \cdot \upsilon_i^{-1} \cdot B_i^{-1} \cdot S_i \quad (1)$$

where B_i is a temperature factor which accounts for the intensity contribution of excited vibrational states, and is represented by the Boltzmann distribution:

$$B_i = 1 - \exp\left(-\frac{h\upsilon_i c}{kT}\right) \quad (2)$$

In Eq. (1), υ_0 is the wavenumber of the laser excitation line ($\upsilon_0 = 18{,}797\ cm^{-1}$ which corresponds to the wavelength of 532 nm), υ_i is the wavenumber of normal mode (cm^{-1}), while S_i is the Raman scattering activity of the normal mode Q_i. The theoretical Raman intensity, I_i^R, is given in arbitrary units (C is a constant equal to 10^{-12}). In Eq. (2) h, k, c, and T are the Planck and Boltzmann constants, speed of light and temperature in Kelvin, respectively. The value of factor B_i was assumed to be 1. Otherwise, the calculated Raman intensities for the bands below 300 cm^{-1} were extremely overestimated in comparison to the experiment [34].

3. Results and discussion

3.1. Conformational analysis

The obtained geometrical parameters of fisetin (bond lengths, bond angles, and torsional angles), calculated by using M052X/6-311+G (2df, p) level of theory, are presented in Table 1. In order to determine the preferred relative positions between the rings B and C the conformational space of the structure presented in Fig. 1 is explored as a function of torsional angle τ between those rings (Fig. 2). It is found that fisetin has a non planar geometry with the part of the molecule, containing cycles A and C, which has complete planarity. In order to examine potential energy surface, the torsion angle τ was scanned in steps of 10° without constraints on all other geometrical parameters. Removing constrain for the torsional angle τ the conformational absolute minimum is found at $\tau = 11.64°$, followed by a relative minimum at $\tau = 168.82°$ with energy difference of only 0.38 kcal mol^{-1}. This result is in a good agreement with the result obtained by the PM3 method (166°) [35], while the results obtained by B3LYP/6-311++G (d, p) method point to planar molecular structure [20].

The maximum of the potential energy lies at $\tau = 90°$ and the introversion barrier between the two minima is about 4.76 kcal mol^{-1} (Fig. 2). This value is almost 1 kcal mol^{-1} lower than one obtained by the B3LYP method [20]. It is worth mentioning that in going from $\tau = 0°$ to $\pm 30°$, the potential energy curve is very flat with an energy variation of about 0.29 kcal mol^{-1} indicating the planar conformation as the one easily obtained, requiring a negligible amount of energy. This result is in good agreement with value obtained by PM6 method (0.17 kcal mol^{-1}) [35].

The results of NBO analysis of the most stable structure of fisetin indicate strongly localized double bonds at the C2–C3 and C4–O positions of the ring C. The bond order values suggest a highly independent electronic delocalization in the rings B and A, which is also one of the main structural features implicated in antioxidant activity of flavon-3-ols. Almost planar structure of fisetin (Fig. 1) enables such electronic delocalization. The C2–C1′ bond lies in the chromone plane, because the torsional angle τ is 168.8° and its length is 1.464 Å. The bond order of this bond, obtained by the NBO analysis, is close to 1 indicating very small conjugation across all the rings of the π system. The positions of the double bonds in the ring C around the carbonyl group indicate a crossconjugated system

Table 1
Bond lengths (Å) and angles (°) of fisetin calculated by the M052X method with 6-311+G(2df,p) basis set.

Bond length	Value	Bond length	Value	Bond angle	Value	Bond angle	Value
D(O1–C2)	1.366	D(C4′–C5′)	1.380	A(O1–C2–C3)	119.90	A(C5′–C6′–C1′)	120.00
D(C2–C3)	1.352	D(C5′–C6′)	1.385	A(C2–C3–C4)	121.8	A(C6′–C1′–C2′)	119.16
D(C3–C4)	1.454	D(C6′–C1′)	1.394	A(C3–C4–C10)	115.68	A(C6′–C1′–C2)	121.76
D(C4–C10)	1.445	D(C2–C1′)	1.464	A(C4–C10–C5)	122.20	A(C2–C3–O3)	123.94
D(C5–C10)	1.398	D(O3–C3)	1.349	A(C10–C5–C6)	120.53	A(C3–C4–O4)	119.04
D(C5–C6)	1.370	D(O4–C4)	1.228	A(C5–C6–C7)	119.52	A(C2′–C3′–O3′)	119.90
D(C6–C7)	1.403	D(O7–C7)	1.354	A(C6–C7–C8)	121.18	A(C3′–C4′–O4′)	115.60
D(C7–C8)	1.378	D(O4′– C4′)	1.367	A(C7–C8–C9)	118.38	A(C6–C7–O7)	121.44
D(C8–C9)	1.388	D(C3′– O3′)	1.356	A(C8–C9–C10)	121.57	t(O1–C2–C1′–C2′)	11.641
D(C9–O1)	1.348	D(O7-H)	0.960	A(C9–O1–C2)	121.84		
D(C9–C10)	1.390	D(O3′-H)	0.963	A(C1′-C2′–C3′)	120.63		
D(C1′–C2′)	1.398	D(O4′-H)	0.959	A(C2′–C3′–C4′)	119.72		
D(C2′–C3′)	1.377	D_H(O3′-H–O4′)	2.145	A(C3′–C4′–C5′)	120.11		
D(C3′–C4′)	1.393	D_H(O4–H-O3)	1.991	A(C4′–C5′–C6′)	120.39		

[36] in which the delocalization is allowed only between C and A or C and B rings but not between the rings A and B. This fact is indirectly confirmed by the investigation in which biphenol molecules were found to be neither completely planar nor conjugated [36].

As peviously reported [20], in the most stable structural (planar) form (Fig. 1), the molecule of fisetin is completely conjugated and all hydroxyl groups are oriented in a way to form the maximum number of internal hydrogen bonds (IHB). Three IHBs are located between the C3–OH and C4–O carbonyl groups, ortho hydroxyl groups in the B ring, and between the C3–OH and C6′–H which has additional stabilizing effect. The conformations lacking these bonds are less stable with respect to the absolute minimum.

3.2. IR and Raman spectral analyses

Experimentally obtained, theoretically calculated and scaled band wavenumbers along with the corresponding assignments for the first 67 (of 84) vibrational modes, appearing in the 4000–400 cm^{-1} region, are presented in Table 2 . Table 2 also lists calculated IR and Raman intensities, potential energy distribution (PED) values and the description of the largest vibrational contributions to the normal modes. It can be noticed that the calculated band positions provide very good fit to the observed results indicating correct mod assignments and scaling factor.

As fisetin possesses very low symmetry, belonging to the C1 symmetry group, its FT-IR and Raman band wavenumbers (Table 2, Fig. 3a and b) are very close with also similar vibrational modes assignments. It is also evident that there are less bands present in the Raman spectrum which is the consequence of the Raman scattering effect itself.

The most distinct and easily recognizable broad bands in IR and NR spectra of phenols and polyphenols (and alcohols when analyzed) are the bands assigned to different modes of O–H vibrations (Table 2). Although being predicted by DFT as sufficiently intense (especially DFT calculated IR intensities) (Table 2) the multiple bands of O–H stretching modes are not observed in the 3700–3450 cm^{-1} region of neither IR (Fig. S1) or Raman spectra of fisetin. In this region only one, very intense IR band at 3415 cm^{-1} (Fig. S1) is present. Due to rather significant difference in wavenumber compared to DFT predicted values, this band could be no closer assigned but to mode 81 belonging to O–H stretching vibration (3-OH) of the ring C. Although the high wawenumber region is also very characteristic to various C–H stretching modes in the experimentally obtained spectra no bands are observed (Fig. S1). The lack in the bands readily assignable to the various O–H and C–H stretching modes could arise from the possible interactions of adjacent molecules in the crystal phase [37,38] or could prove supposed intramolecular hydrogen-bonded compound [20]. The largest vibrational contributions to the normal stretching modes (PED values) (Table 2) in the 3700–3000 cm^{-1} region are assigned almost solely to the stretching modes themselves while the rest of the modes are presented as the combination of various contributions.

The most intense bands of the spectra are to be found in the 1650–1500 cm^{-1} wavenumber region. As in the other flavone derivatives [37–41] this IR region involves a combination of the

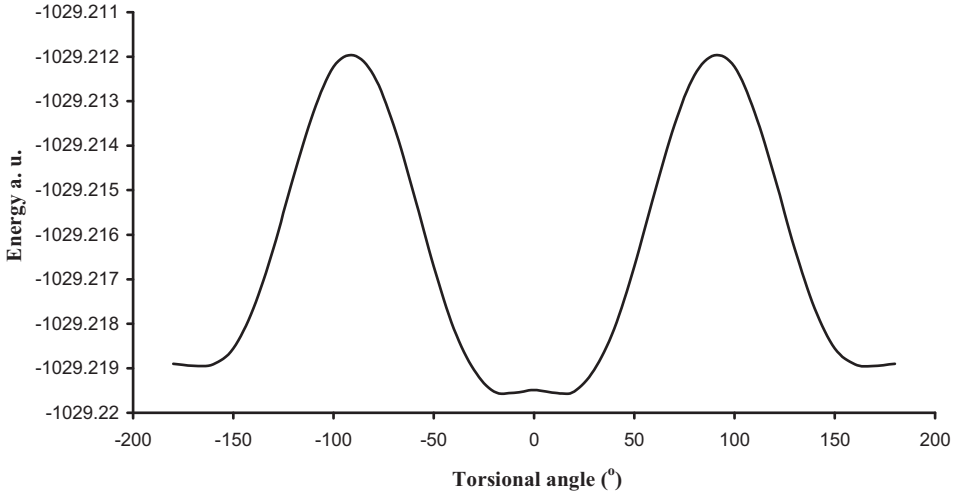

Fig. 2. Rotation barrier around the internal bond C2–C1′ calculated with the M052X/6-311+G (2df, p) method for fisetin.

Table 2
Experimental and calculated wavenumbers of the bands in the IR and Raman spectra of fisetin, assigments and intensities[a] of the normal modes.

Mode	Mode assignments	Experimental values		M052X/6-311+G(2df,p)					
		ν_{IR} (cm^{-1})	ν_{Raman} (cm^{-1})	Unscaled freq. (cm^{-1})	Scaled freq. (cm^{-1})	IR intensity	Raman intensity	Raman activity	PED (%)
84	OH stretching (A)			3920.24	3702.27	45.84	14.48	215.40	ν_{OH} (100)
83	OH stretching (B) (4′-OH)			3911.57	3694.09	43.82	10.68	158.92	ν_{OH} (100)
82	OH stretching (B) (3′-OH)			3866.08	3651.13	46.03	5.86	87.23	ν_{OH} (100)
81	OH stretching (C) (3-OH)	3415		3657.70	3454.33	54.94	8.63	128.44	ν_{OH} (100)
80	CH stretching (B)			3286.82	3104.07	2.21	1.96	29.11	ν_{CH} (99)
79	CH stretching (A)			3264.90	3083.37	0.64	2.46	36.54	ν_{CH} (99)
78	CH stretching (B)			3257.93	3076.79	0.38	4.28	63.74	ν_{CH} (99)
77	CH stretching (A)			3236.31	3056.37	0.82	6.28	93.49	ν_{CH} (93)
76	CH stretching (A)			3213.35	3034.69	3.42	8.79	130.82	ν_{CH} (99)
75	CH stretching (B)			3209.10	3030.67	1.47	9.39	139.64	ν_{CH} (94)
74	C2═C3 stretching (C) C═O stretching (C) COH bending (C) (3-OH)		1658	1743.12	1646.20	14.15	32.58	484.70	ν_{CC} (64) + $\nu_{C=O}$ (11)
73	CC stretching (A) C2═C3 stretching (C) C═O stretching (C)		1635	1726.10	1630.13	86.83	14.92	222.02	ν_{CC} (53)
72	CC stretching (A, B) C═O stretching (C) OC stretching (B)	1618	1618	1713.20	1617.95	100.00	8.65	128.64	ν_{CC} (59)
71	OC stretching (B) C═O stretching (C) CC stretching (B, A, A–C)			1707.00	1612.09	69.58	100.00	1487.70	ν_{OC} (28)
70	CC stretching (B)	1596		1690.34	1596.36	55.38	22.92	340.95	ν_{CC} (61)
69	CC stretching (A, A–C) CC stretching (C) (C2═C3) C═O stretching (C)	1570	1570	1669.35	1576.53	12.69	43.68	649.87	ν_{CC} (61)
68	CO stretching (B) CC stretching (B)	1504	1506	1591.68	1503.18	57.64	2.61	38.85	ν_{CO} (38) + ν_{CC} (29)
67	HCC bending (A)		1475	1579.22	1491.42	21.44	0.81	12.07	δ_{HCC} (12) + ν_{CC} (24)
66	CO stretching (A–C) CC stretching (A)	1443	1440	1535.63	1450.25	85.74	0.89	13.27	ν_{CO} (25)
65	COH bending (B) HCC bending (B) CCC bending (B) CCO bending (A)	1420	1411	1523.34	1438.64	1.95	0.71	10.57	δ_{COH} (15) + δ_{HCC} (11) + δ_{CCC} (10)
64	CCO bending (C) COH bending (C)	1386	1391	1473.17	1391.26	93.50	31.71	471.69	ν_{CO} (15) + δ_{CCO}(26) + δ_{HOC} (13)
63	CC stretching (A) COH bending (A) (7-OH) COH bending (C) (3-OH)		1342	1426.96	1347.62	2.72	3.44	51.20	ν_{CC} (71)

62	CC stretching (B) COH bending (B) (3′-OH; 4′-OH)	1320	1314	1396.88	1319.21	9.11	6.51	96.79	ν_{CC} (45)
61	COH bending (C) (3-OH) HCC bending (B)			1379.26	1302.57	75.15	31.00	461.14	δ_{COH} (37) + δ_{HCC} (10) + ν_{CC} (21)
60	HCC bending (B)	1280		1364.52	1288.65	39.68	0.56	8.36	δ_{HOC} (14) + δ_{HCC} (33)
59	COH bending (B) (3′-OH; 4′-OH) CCO bending (B)		1273	1350.64	1275.54	29.81	3.65	54.25	δ_{COH} (15) + δ_{HCC} (19) + δ_{HCC} (11)
58	CC stretching (A, B) CO stretching (A)			1335.40	1261.15	78.00	3.65	54.36	δ_{COH} (13) + ν_{CC} (27)
57	CC stretching (A, A–C) CO stretching (A, B)	1245		1328.01	1254.17	72.29	1.80	26.74	ν_{CC} (57)
56	CC stretching (A, B, C) HCC bending (A, B) COH bending (C, B)		1228	1299.82	1227.55	20.04	0.37	5.56	ν_{OC} (25) + δ_{HCC} (13)
55	CO stretching (A, C) COH bending (A) (7-OH)	1200	1196	1262.96	1192.74	47.81	0.55	8.25	ν_{OC} (38) + δ_{COH} (13)
54	CO stretching (A, B, C) CC stretching (C, A, C–A) HCC bending (A)		1177	1253.87	1184.15	2.12	0.42	6.23	ν_{CO} (12)
53	CC stretching (C) CO stretching (A, B) COH bending (A, B) HCC bending (A, B)	1167		1236.04	1167.32	1.14	0.33	4.86	ν_{CO} (20)
52	HCC bending (B) COH bending (B, A)			1223.60	1155.57	65.33	1.39	20.62	δ_{COH} (54) + ν_{CO} (11)
51	COH bending (A) HCC bending (A, B)	1135		1187.93	1121.88	22.88	2.06	30.68	δ_{HCC} (11) + δ_{COH} (25)
50	HCC bending (B) COH bending (B) (4′-OH)	1112		1186.85	1120.86	65.46	1.20	17.78	δ_{CCC} (12) + ν_{CC} (18) + δ_{HCC} (38)
49	HCC bending (A)	1097	1097	1167.94	1103.00	35.23	0.05	0.71	δ_{HCC} (54)
48	HCC bending (A)			1151.27	1087.26	47.93	2.85	42.42	δ_{COH} (41) + δ_{CCC} (11)
47	COH bending (B) CCC bending (B)			1141.25	1077.80	3.99	0.10	1.44	δ_{CCC} (23) + δ_{HOC} (44)
46	CCO bending (C–B) HCC bending (B) CCC bending (B)	1014	1016	1059.93	1001.00	9.96	2.96	44.01	δ_{CCC} (20)
45	CCCH torsion (A)	976	973	1009.76	953.62	0.17	0.01	0.17	τ_{CCCH} (73)
44	CCC bending (A)			1003.12	947.35	7.51	0.74	10.96	δ_{CCC} (23)
43	CCC bending (A, B, C) COH bending (C)	933		983.99	929.28	0.03	0.02	0.23	δ_{HCC} (12) + δ_{CCC} (28)
42	HCCH torsion (B)		932	975.31	921.08	3.24	1.49	22.19	τ_{HCCC} (75)
41	HCCC bending (B)	880		933.52	881.62	6.69	0.05	0.80	τ_{HCCC} (80)

Table 2 (*Continued*)

Mode	Mode assignments	Experimental values		M052X/6-311+G(2df,p)					
		ν_{IR} (cm^{-1})	ν_{Raman} (cm^{-1})	Unscaled freq. (cm^{-1})	Scaled freq. (cm^{-1})	IR intensity	Raman intensity	Raman activity	PED (%)
40	HCCC bending (A)	851	849	899.82	849.79	10.20	0.02	0.27	τ_{HCCC} (51) + τ_{CCCC} (36)
39	CCC bending (B) COC bending (C)	836		863.62	815.60	5.96	0.29	4.26	δ_{HCC} (44) + ν_{CO}(11)
38	HCCC torsion (A)	807		858.60	810.86	2.89	0.01	0.18	τ_{HCCC} (39) + τ_{OCCC} (25)
37	HCCC torsion (B)	787	792	848.96	801.76	9.18	0.05	0.75	τ_{HCCC} (75)
36	CO stretching (B) CC stretching (B)	775		821.14	775.48	18.15	2.85	42.33	ν_{OC} (68)
35	OCCC torsion (A–C) o.p. OCCC torsion (A) o.p.	755	756	811.00	765.91	11.37	0.07	0.99	τ_{OCCC} (o.p.) (37) + τ_{CCCC} (25)
34	CC stretching (A) CCC bending (A)			783.49	739.93	0.41	1.20	17.87	δ_{CCC} (33)
33	CCCC torsion (A, B) OCCC torsion (B) o.p. CCOC torsion (C–B) o.p.	723	724	757.42	715.31	0.25	0.18	2.60	τ_{CCCC} (44)
32	CCCC torsion (A, C-B) CCOC torsion (A-C, C-B) o.p. OCCC torsion (C, B) o.p. CCCC torsion (C–B) o.p.	701	697	736.62	695.66	2.21	0.05	0.77	τ_{OCCC} (o.p.) (12) + τ_{HCCC} (19) + τ_{CCCC} (36)
31	CCO bending (B, C)	671	672	714.90	675.15	2.05	0.13	1.99	ν_{OC} (13) + δ_{CCO} (44) + δ_{COC} (10)
30	CCOC torsion (C-B) o.p. CCCC torsion (B) o.p. OCCC torsion (B) o.p. CCCC torsion (A)			693.76	655.19	0.34	0.29	4.36	τ_{CCCC} (10) + τ_{CCOC} o.p. (31)
29	OC stretching (A, B) CC stretching (A, B, C)			685.07	646.98	2.27	0.54	8.09	ν_{CC} (11) + δ_{CCO} (11)
28	OCCC torsion (A) o.p. CCOC torsion (A) o.p.	622	625	657.31	620.76	0.78	0.07	1.02	τ_{HCCC} (11) + τ_{OCCC} o.p. (64)

27	CCC bending (B) CCO bending (C, B) CCC bending (C–B)			635.38	600.05	8.77	0.05	0.80	δ_{CCO} (31)
26	HOCC torsion (C)	586	586	631.18	596.09	29.26	0.08	1.16	τ_{HOCC} (72)
25	CCO bending (B) CCC bending (B)	568	567	601.11	567.69	0.21	0.56	8.36	δ_{CCO} (10) + δ_{CCC} (40)
24	CCC bending (B) CCO bending (A–C, B)	554		596.45	563.29	8.21	0.62	9.27	δ_{CCO} (11) + δ_{CCC} (46)
23	CCOC torsion (C–B) o.p. CCCC torsion (B)	524	524	573.82	541.92	0.64	0.11	1.67	τ_{HOCC} (10) + τ_{CCOC} (37)
22	CCC bending (A, A–C) CCO bending (A–C)	480		520.32	491.39	0.19	1.30	19.41	δ_{CCO} (18) + δ_{CCC} (12)
21	CCO bending (B) CCC bending (B) COH bending (B)	449		483.57	456.68	1.56	0.06	0.95	δ_{CCO} (52)
20	CCCC torsion (A) OCCC torsion (A) o.p. CCOC torsion (A–C) o.p.		446	477.08	450.55	1.30	0.07	1.07	τ_{CCCC} (56) + τ_{OCCC} (11)
19	OCCC torsion (B) o.p. CCCC torsion (B)	433		463.36	437.60	0.09	0.08	1.17	τ_{OCCC} o.p. (61)
18	CCO bending (A, A–C) CCC bending (A)			447.85	422.95	0.14	0.05	0.80	δ_{CCO} (35) + δ_{CCC} (11)
17	OCCC torsion (C) o.p.	405		417.69	394.47	1.12	0.14	2.01	τ_{OCCC} o.p.(56)

Raman activity = Si of the normal mode; o.p. – out of plane vibrations.

[a] IR intensities are normalized with highest peak equal to 100; Raman intensities are calculated using the formulae for Raman intensity and after that are normalized to 100.

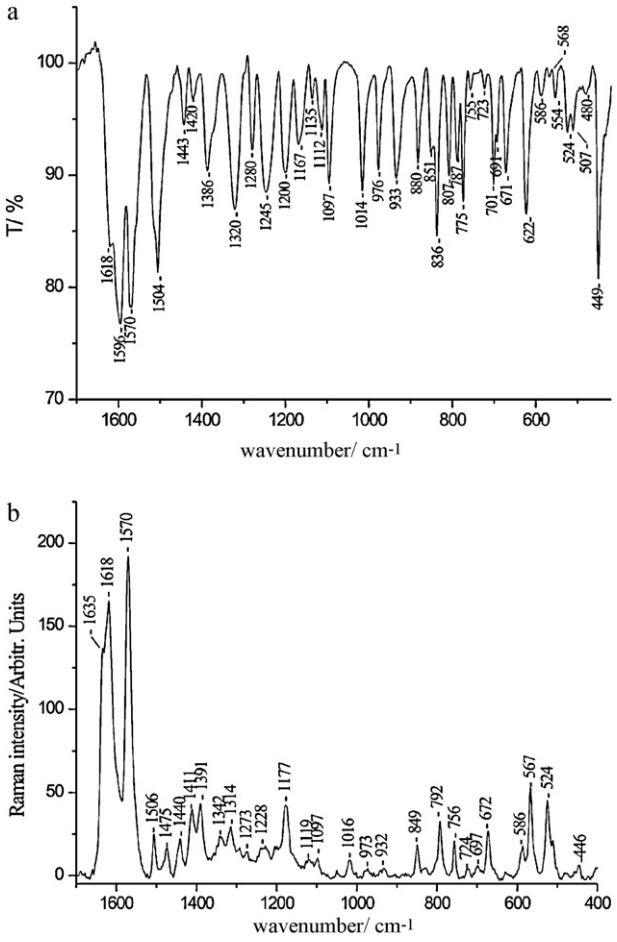

Fig. 3. The 1700–400 cm^{-1} region of the IR (a) and Raman (b) spectra of fisetin.

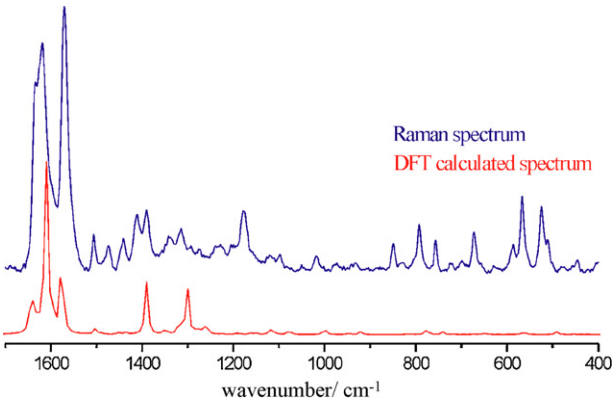

Fig. 4. Raman spectrum of fisetin and comparison with density functional calculation in the 1700–400 cm^{-1} region. Spectra are translated vertically in order to be viewed clearly.

C=O stretching (1618 and 1570 cm^{-1}) (modes ν_{72} and ν_{69}), C2=C3 stretching (1570 cm^{-1}) (ν_{69}) and C–C stretching (1618, 1596, 1570, 1504 cm^{-1}) modes (ν_{72}, ν_{70}, ν_{69} and ν_{68}) (Table 2, Fig. 3a). In the Raman spectrum these bands, also as the most intense, appear in the 1630–1500 cm^{-1} region, almost at the same positions as corresponding bands in the IR spectrum (1635, 1618 and 1570 cm^{-1}; 1635 and 1570 cm^{-1}; 1635, 1618 and 1570 cm^{-1}) (Table 2, Fig. 3b).

As fisetin belongs to the class of flavonols, 3-OH flavones, the frequencies of the most intense bands assigned to both the C=O and C2=C3 stretching modes (ν_{72} and ν_{69}) are little bit decreased and positioned at lower values compared to flavanone (1695 cm^{-1}), flavone (1649 cm^{-1}), and 5-OH flavone (1657 cm^{-1}) [37,38]. It has been suggested that frequency decrease results from the increased conjugation of the carbonyl group with the pyrone ring through the C2=C3 bond [37,38].

The bands between 1500 and 1000 cm^{-1} mostly involve C–C stretching, O–C stretching and in-plane C–C–H, C–O–H, C–C–O and C–C–C bending vibrations of the rings. The most intense bands in this region assign modes ν_{62}, ν_{57}, ν_{55}, ν_{49} and ν_{46}. Medium intensity bands assign modes ν_{64}, ν_{60}, ν_{53} and ν_{50} while low intensity bands belong to ν_{65} and ν_{51} modes. The plurality of medium to low intensity bands which appear below 1000 cm^{-1} (ν_{45}–ν_{17}) is predominantly assigned to the C–O–H, C–C–O, H–C–C, C–C–C and C–O–C bending modes of all three rings. This region is also characteristic to the combination of in plane C–C–C–H, H–C–C–H, C–C–C–C, C–C–O–C and out of plane O–C–C–C, C–C–O–C and C–C–C–C torsional modes.

The intensity distribution in the 1500–1000 cm^{-1} Raman region does not coincide with the intensity distribution of the corresponding bands in the IR region (Fig. 3a and b). The most intense bands belong to ν_{73}, ν_{72} and ν_{69} modes, medium intensity bands to ν_{68}, ν_{67}, ν_{65}, ν_{64} and ν_{54} modes while the modes ν_{63}, ν_{56}, ν_{49} and ν_{46} are low in intensity.

In almost whole wavenumber region an excellent match of the experimentally obtained spectra with the DFT calculated modes is obtained. Only a few of the calculated wavenumbers do not match the observed ones in the low wavenumber region (below 1000 cm^{-1}), such as modes ν_{45}, ν_{39}, ν_{23}. The fact that the signal-to noise ratio in the low wavenumber region is low might explain this discrepancy.

Although the DFT calculated band positions provide very good fit to the observed values, indicating correct mod assignments (Table 2), the predicted DFT band intensities (both IR and Raman) do not coincide with the experimental values (Table 2, Fig. 4) especially in the low frequency region.

3.3. *Comparative analysis of the spectra*

The comparative analysis of fisetin spectrum and the spectra of structurally related flavones, baicalein (5,6,7-trihydroxyflavone) and quercetin (3,5,7,3′,4′-pentahydroxyflavone) (Fig. S2), is performed in order to additionally validate the assignment of the bands. The comparison is focused on selected regions of the spectra which are of particular interest in structural changes of flavones. Very important O–H stretching region (3900–3640 cm^{-1}) is not analyzed because of the lack of the bands in the experimentally obtained spectra of fisetin.

The most interesting region of fisetin spectra refers to combination of the C=O stretching (modes ν_{72} and ν_{69}), C2=C3 stretching (ν_{69}) and C–C stretching (ν_{72}, ν_{70}, ν_{69} and ν_{68}) vibrational modes. The comparison of the 1700–1000 cm^{-1} Raman regions of fisetin and baicalein spectra is presented in Fig. 5. The discriminant bands are labeled with the wavenumbers. Table S1 lists experimental and calculated positions of the bands in the IR and Raman spectra of baicalein. Fig. 5 presents quite good match between modes ν_{72} (1618, 1618 and 1618 cm^{-1}) (IR, Raman and predicted by DFT, respectively), ν_{70} (1596, –, and 1596 cm^{-1}) and the mode ν_{69} (1570, 1570, and 1576 cm^{-1}) in the spectra of fisetin with the modes ν_{73} (1615, 1612 and 1620 cm^{-1}) (IR, Raman and predicted by DFT, respectively), ν_{71} (1587, 1589, and 1593 cm^{-1}) and the mode ν_{70} (1560, 1566 and 1567 cm^{-1}) in the spectra of baicalein (Table S1). It is worth pointing out that the wavenumbers of both the modes ν_{69} in the spectra of fisetin and baicalein do not differ substantially as might be expected. Taking account the fact that fisetin

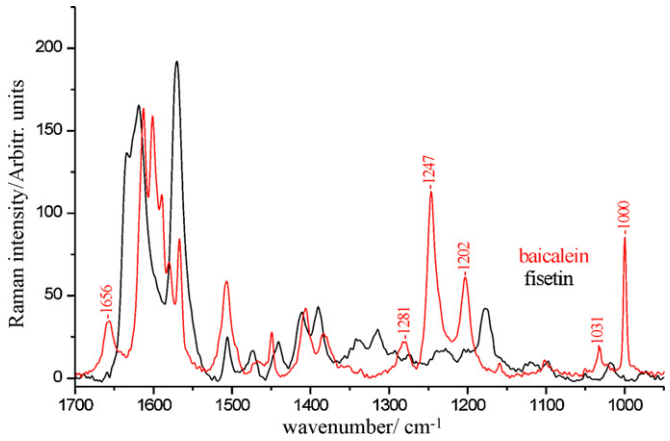

Fig. 5. Comparison of the 1700–1000 cm^{-1} Raman region of fisetin and baicalein spectra. The discriminant bands are labeled with the wavenumbers.

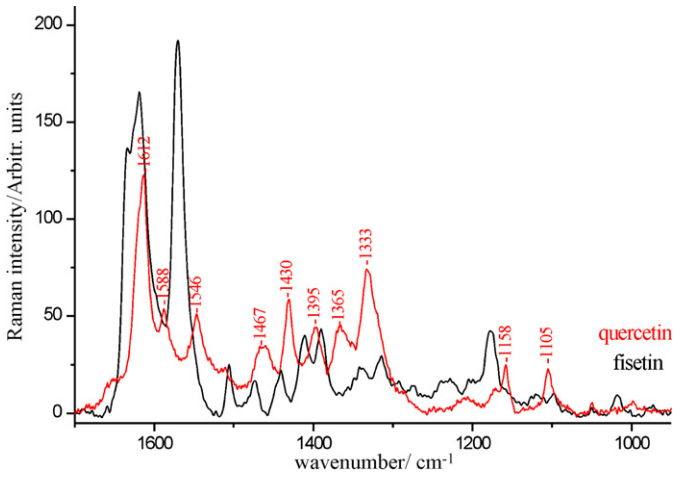

Fig. 6. Comparison of the 1700–1000 cm^{-1} Raman region of fisetin and quercetin spectra. The discriminant bands are labeled with the wavenumbers.

is C3–OH substituted molecule and baicalein is not it could be expected that the substitution of the C3 position, which is an important part of the unperturbed vibration of the unsubstituted C ring, would decrease the wavenumber of the lines attributed to C=O and C2=C3 stretching. The band at 1656 cm^{-1} (ν_{74}) present in the spectrum of baicalein (Table S1), assigned to the combination of C=O and C–C stretching modes of the rings A and C, has match in very weak band at 1658 cm^{-1} in the spectrum of fisetin (Table 2). This band, also assigned to the combination of C=O and C2=C3 stretching modes, participate with the small percentage in the predicted PED values. The difference between the frequences of ν_{74}, in the spectrum of baicalein, and ν_{72}, in the spectrum of fisetin, could be explained by adding a substantial component of the C–O–H bending vibrations to the normal mode which are also a part of a predicted PED values for this particular mode (Table S1). A part of this is simply due to the fact that there are three hydroxyl groups in the A ring of baicalein which certainly attribute the vibrational modes of the substituted ring. The discriminant bands in the spectrum of baicalein (Fig. 5) further point to the structural features by which fisetin and baicalein differ. The bands at 1281 and 1000 cm^{-1} point to the difference in the C–C–H bending vibrations of the ring B. The bands at 1247 and 1031 cm^{-1}, assigned to C6–OH and C7–OH bending vibrations of the ring A, clearly indicate the difference in the A ring substitution pattern. The band at 1202 cm^{-1}, assigned to C2–C1′ stretching vibration between the rings C and B, indicate the difference in the structure of the ring B.

The most intense band in the Raman spectrum of solid quercetin (Fig. 6) is that at 1612 cm^{-1}, which is assigned to the combination of the C2=C3 stretching and in-plane C3–OH and C5–OH bending modes [38]. Less intense bands at 1588 and 1546 cm^{-1} are assigned as the C=O stretch, C5–OH in plain bending of the ring A and C–C stretching of the ring B. The most discriminant bands are in the 1470–1330 cm^{-1} region which clearly establishes the difference in the A and B rings substitution patterns. The band at 1467 cm^{-1} assign the combination of C3–OH, C5–OH and C7–OH in plain bending and C6–C8–H bending modes, the band at 1430 cm^{-1} assign C3–OH and C5–OH in plain bending modes while the band at 1395 cm^{-1} is also assigned to C3–OH, C5–OH and C7–OH in plain bending modes. The bands at 1365 cm^{-1} (C3–OH, C5–OH and C7–OH in plain bendings of the ring A), 1333 cm^{-1} (C3–OH in plain bending of the ring C), 1158 cm^{-1} (C7–OH and C–C–H bendings of the ring A) and 1105 cm^{-1} (C3–OH, C3′–OH, C4′–OH and C–C–H bend) also point to the difference in structure.

4. Conclusion

The results of the applied M05-2X/6-311+G (2df, p) density functional method in determination of the spectroscopic and electronic features of fisetin point to non-planar molecule, characterized by an extended delocalization and conjugation of the *p* electrons. The detailed vibrational spectral analysis and the assignments of the bands, done on the best-fit basis comparison of the experimentally obtained and theoretically calculated IR and Raman spectra, match quite well indicating DFT calculations as very accurate source of normal mode assignments. Comparative hydroxylation pattern analysis could provide good insight into the structural changes which appear upon all relevant fisetin interactions.

Acknowledgements

The authors acknowledge financial support by the Ministry of Science of Republic of Serbia (Grant No. 172015). The authors would also like to thank Prof. Jamróz MH for VEDA 4 programme.

Appendix A. Supplementary data

Supplementary data associated with this article can be found, in the online version, at doi:10.1016/j.saa.2011.08.001.

References

[1] J.B. Harborne, C.A. Williams, Phytochemistry 55 (2000) 481–504.
[2] C. Santos-Buelga, M.T. Escribano-Bailon, V. Lattanzio, in: Santos-Buelga, Escribano-Bailon, Lattanzio (Eds.), Recent Advances in Polyphenol Research, Wiley-Blackwell, 2010.
[3] C. Kandaswami, E. Middleton, Adv. Exp. Med. Biol. 366 (1994) 351–376.
[4] A. Beretz, R. Anton, J. Cazenave, Plant Flavonoids in Biology and Medicine 11: Biochemical, Cellular, and Medicinal Properties, Alan R. Liss, New York, USA, 1988.
[5] D.F. Brit, S. Hendrich, W. Wang, Pharmacology and Therapeutics 90 (2–3) (2001) 157–177.
[6] J.P. Brown, Mutat. Res. 75 (3) (1980) 243–277.
[7] W.S. Chang, Y.L. Lee, F.J. Lu, H.C. Chang, Anticancer Res. 13 (6A) (1993) 2165–2170.
[8] L. Cipak, P. Rauko, E. Miadokova, I. Cipakova, L. Navotny, Leuk. Res. 27 (1) (2003) 65–72.
[9] N.P. Das, Flavonoids in Biology and Medicine III-Current Issues in Flavonoids Research, Singapore University Press, Singapore, 1990, p. 213.
[10] C.V. De Whalley, S.M. Rankin, J.R.S. Hoult, W. Jessup, D.S. Leake, Biochem. Pharmacol. 39 (11) (1999) 1743–1750.
[11] W. Ren, Z. Qian, H. Wang, L. Zhu, L. Zhang, Med. Chem. Res. 23 (4) (2003) 519–534.
[12] N.C. Cook, S.J. Samman, Nutr. Biochem. 7 (1996) 66–76.

[13] L.R. Fukumoto, G.J. Mazza, J. Agric. Food Chem. 48 (2000) 3597–3604.
[14] L.H. Yao, Y.M. Jiang, J. Shi, N.F.A. Tomas-Barberan, N. Datta, R. Singanusong, Plant Foods Hum. Nutr. 59 (2004) 113–122.
[15] R.J. Nijveldt, E. Nood, D.E.C. Hoorn, P.G. Boelens, K. Norren, P.A.M. Leeuwen, Am. J. Clin. Nutr. 74 (4) (2001) 418–425.
[16] V. Cody, E. Middleton, J.B. Harborne, Plant Flavonoids in Biology and Medicine: Biochemical, Pharmacological, and Structure–Activity Relationships, A. R.Liss Incorporated, New York, 1986.
[17] V. Cody, E. Middleton, J.B. Harborne, A. Beretz, Plant Flavonoids in Biology and Medicine II: Biochemical, Cellular, and Medicinal Properties, A.R. Liss Incorporated, New York, 1988.
[18] R.A. Larson, Naturally Occurring Antioxidants, Lewis Publishers, CRC Press LLC, Boca Raton, 1997.
[19] P.G. Pietta, in: C.A. Rice-Evans, L. Packer (Eds.), Flavonoids in Health and Disease, M. Dekker Inc, New York, 1997.
[20] Z.S. Marković, S.V. Mentus, J.M. Dimitrić Marković, J. Phys. Chem. A 113 (2009) 14170–14179.
[21] Z.S. Marković, J.M. Dimitrić Marković, D. Milenković, N. Filipović, J. Mol. Model. (2011), doi:10.1007/s00894-010-0942-y.
[22] Z.S. Marković, J.M. Dimitrić Marković, Ć.B. Doličanin, Theor. Chem. Acc. 127 (2010) 69–80.
[23] D.A. Parthenopoulos, M. Kasha, Chem. Phys. Lett. 146 (1988) 77–82.
[24] D. Gormin, A. Sytnik, M.J. Kasha, J. Phys. Chem. 101A (1997) 672–677.
[25] Y. Zhao, D.G. Truhlar, Theor. Chem. Acc. 120 (2008) 215–241.
[26] M.J. Frisch, G.W. Trucks, H.B. Schlegel, G.E. Scuseria, M.A. Robb, J.R. Cheeseman, V.G. Zakrzewski, J.A. Montgomery Jr., R.E. Stratmann, J.C. Burant, S. Dapprich, J.M. Millam, A.D. Daniels, K.N. Kudin, M.C. Strain, O. Farkas, J. Tomasi, V. Barone, M. Cossi, R. Cammi, B. Mennucci, C. Pomelli, C. Adamo, S. Clifford, J. Ochterski, G.A. Petersson, P.Y. Ayala, Q. Cui, K. Morokuma, A.D. Malick, K.D. Rabuck, K. Raghavachari, J.B. Foresman, J. Cioslowski, J.V. Ortiz, A.G. Baboul, B.B. Stefanov, G. Liu, A. Liashenko, P. Piskorz, I. Komaromi, R. Gomperts, R.L. Martin, D.J. Fox, T. Keith, M.A. Al-Laham, C.Y. Peng, A. Nanayakkara, M. Challacombe, P.M.W. Gill, B. Johnson, W. Chen, M.W. Wong, J.L. Andres, C. Gonzalez, M. Head-Gordon, E.S. Replogle, J.A. Pople, Gaussian 09, Revision A. 1-SMP, Gaussian Inc., Wallingford, CT, 2009.
[27] Y. Zhao, N.E. Schultz, D.G. Truhlar, J. Chem. Phys. 123 (2005), 161103 (1–5).
[28] Y. Zhao, N.E. Schultz, D.G. Truhlar, J. Chem. Theory Comput. 2 (2006) 364–382.
[29] M.H. Jamróz, Vibrational energy distribution analysis: VEDA 4 programme, Warsaw, 2004.
[30] A.E. Reed, R.B. Weinstock, F. Weinhold, J. Chem. Phys. 83 (1985) 735–746.
[31] E.D. Glendening, A.E. Reed, J.E. Carpenter, Weinhold F NBO Version 3.1.
[32] A.E. Reed, L.A. Curtiss, F. Weinhold, Chem. Rev. 88 (1988) 899–926.
[33] J.E. Carpenter, F. Weinhold, J. Mol. Struct. (THEOCHEM) 169 (1988) 41–62.
[34] R. Wysokinsk, K. Hernik, R. Szostak, D. Michalska, Chem. Phys. 333 (2007) 37–48.
[35] Z. Marković, J. Dimitrić-Marković, Ć. Doličanin, J. Serb. Soc. Comp. Mech. 3 (2) (2009) 43–55.
[36] W. Hutter, H.K. Bodenseh, J. Mol. Struct. 291 (1993) 151–158.
[37] Z. Jurasekova, J.V. Garcia-Ramos, C. Domingo, S. Sanchez-Cortes, J. Raman Spectrosc. 37 (2006) 1239–1241.
[38] T. Teslova, C. Corredor, R. Livingstone, T. Spataru, R.L. Birke, J.R. Lombardi, M.V. Cañamares, M. Leona, J. Raman Spectrosc. 38 (2007) 802–818.
[39] Z. Jurasekova, A. Torreggiani, M. Tamba, S. Sanchez-Cortes, J.V. Garcia-Ramos, J. Mol. Struct. 918 (2009) 129–137.
[40] A. Torreggiani, A. Trinchero, M. Tamba, P. Taddei, J. Raman Spectrosc. 36 (2005) 380–388.
[41] A. Torreggiani, Z. Jurasekova, S. Sanchez-Cortes, M. Tamba, J. Raman Spectrosc. 39 (2008) 265–275.